Turkish Journal of Electrical Engineering & Computer Sciences

http://journals.tubitak.gov.tr/elektrik/

Research Article

Turk J Elec Eng & Comp Sci
(2018) 26: 363 – 377

doi:10.3906/elk-1702-215

Field-verified integrated EAF-SVC-electrode positioning model simulation and a novel hybrid series compensation control for EAF

Ahmed HASSAN[1,*], Amr ABOU-GHAZALA[2], Ashraf MEGAHED[2]
[1]Al-Ezz Al-Dekheila Steel Co., Alexandria, Egypt
[2]Department of Electrical Power, Faculty of Engineering, Alexandria University, Alexandria, Egypt

Received: 16.02.2017 • **Accepted/Published Online:** 14.11.2017 • **Final Version:** 26.01.2018

Abstract: In this paper, modeling and simulation of a typical steel-making network are realized using MATLAB Simulink environment and validated using trends collected from an actual steel plant. The models integrate different reactions between an electric arc furnace (EAF), a static Var compensator, and electrode positioning systems according to a previously introduced theory of operations. In addition, the conventional electrode positioning control performance is compared with the new hybrid series compensation control method to demonstrate the superiority of the new method regarding system response. With help of the proposed series compensation, the reference resistance value was restored 2.5 s faster than the conventional method alone for the same disturbance on the electrodes. The improved response speed will be reflected in maximum power transfer to EAF electrodes, minimum on-tap heat time, efficiency of power consumption of electrodes arm positioning system, and consumption per heat of electrodes and refractories.

Key words: Electric arc furnace, static Var compensator, electrodes positioning, power quality, harmonics

1. Introduction

A static Var compensator (SVC) is mandatory for electric arc furnace (EAF) operation. Accurate simulation of EAF would not be complete without a suitable SVC model. The integration of a SVC model with EAF is not readily available in the literature. A more realistic integrated model should also integrate the interaction between network dynamics and the electrode-positioning system, as this interaction is valuable in terms of evaluating flicker level, total harmonic distortion, protection schemes, energy utilization, impact on operating parameters, etc.

A common drawback in the models presented in [1–4] is that the developed models did not combine the interaction between EAF, SVC, and electrode positioner models, as shown in Figure 1. In addition, they were based on deterministic data and hence could not be considered generic models that can represent every arcing stage according to unique independent plant conditions.

Models in [5–7] tackled the electrodes positioning control methods, whether current control or neurofuzzy or something else. Even though these control methods reduced the error in the control signal, whether current or impedance, in a shorter time than older techniques, it did so by inducing large oscillations in all the variables. A large overshoot in the electrode position is particularly undesirable in arc furnace operation [8].

If the scrap steel falls away from the electrode and the electrode position controller induces a large overshoot as it corrects the disturbance, the electrode may strike the steel. Using these regulator types will

*Correspondence: ahmedh@ezzsteel.com.eg

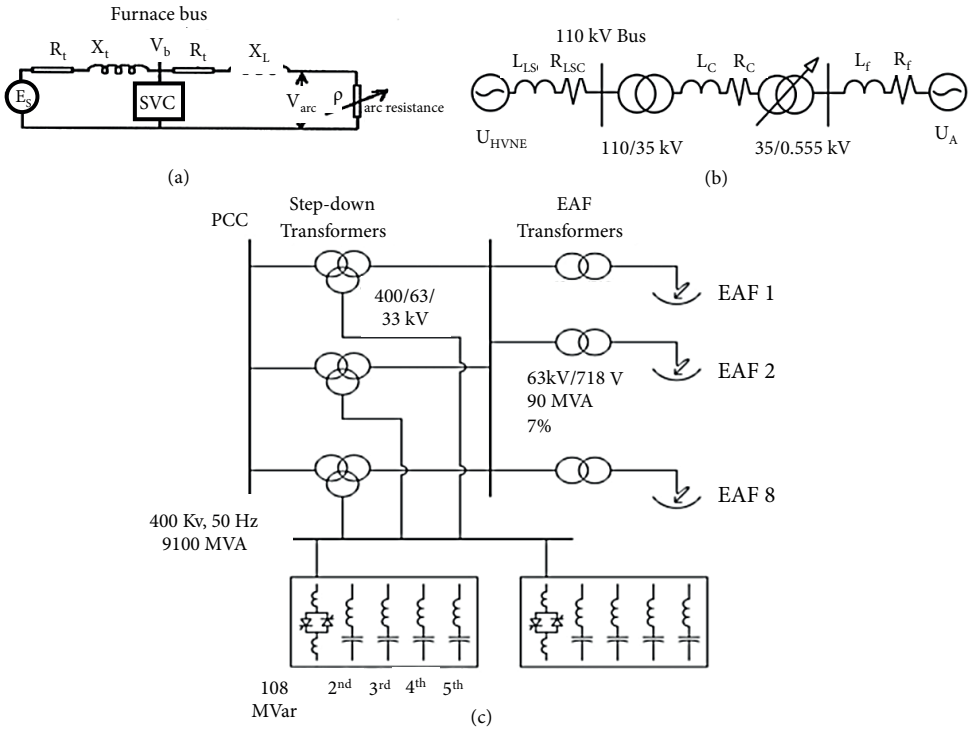

Figure 1. Single line diagrams of isolated models presented in [1], [2], and [4], respectively.

therefore increase the possibility of electrode breakage. Hence, the mechanical response remains the bottleneck that easily destroys any improvement in the performance of any control algorithm.

Several recent studies, such as [9–11], realized this and discussed the usage of supplementary series reactors installed between the substation transformer and the furnace transformer to minimize the on-load tap changer operation and maximize EAF performance without making the furnace power exceed the nominal transformer rating with the higher secondary voltage taps. A higher voltage tap is desirable to reduce the current and consequently the electrode consumption. Since electrode consumption represents up to 10% of the furnace operating cost [12] and it is directly related to the secondary current, the installation of a series reactor helps reduce furnace operating current and hence reduces electrode consumption by up to 20% of the furnace transformation cost [13].

The aim of this paper is to introduce a generic and integrated EAF-SVC-electrode positioner model as shown in Figure 2, compared to the previously introduced isolated models presented in Figure 1. The model is realized using MATLAB Simulink environment and validated using trends collected from an actual steel plant to give realistic representation of the chaotic–dynamic performance of the EAF. This generic model will help to fill in the gaps in the previous literature that are indicated above. In addition, a new hybrid series-impedance control concept is introduced that eliminates the bottleneck of the mechanical system response by using active series resistance control that works in conjunction with the electrode positioning controllers to increase the speed of disturbance clearance electrically without the need to impose large oscillations on the mechanical system.

2. Proposed algorithm theory of operation

Considering the integrated EAF-SVC-electrode positioning analysis scheme model shown in Figures 2 and 3, respectively, if the power input falls below the optimum operating point, the energy input to the furnace is

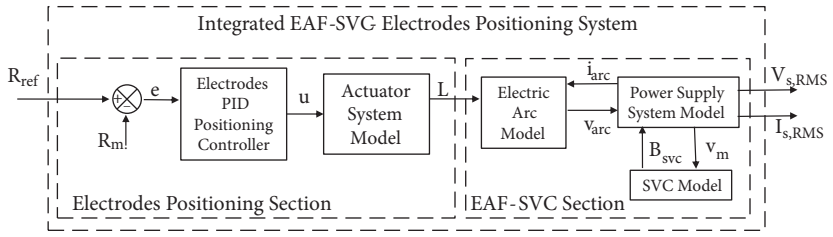

Figure 2. Analysis scheme of integrated EAF-SVC-electrode system model.

inefficiently utilized. To clear this disturbance, the electrode-position controllers operate in response to an error (e) between the impedance variable (R_m) and its reference value (R_{ref}) to adjust the electrode positions by lowering the electrode. This control action decreases EAF secondary circuit impedance and reestablishes the desired power input, where L is the electrode's mast displacement in millimeters and it is assumed proportional to arc resistance. Alternatively, if the power input increases or moves to the right of the operating point and the furnace is operating on a high voltage tap, the refractories may be damaged by radiation from the arcs and the transformer will be overloaded [8]. Again, the electrode-position controllers operate in response to the error between the impedance variable and its reference value, to adjust the electrode positions by raising the electrode. This control action will increase EAF secondary circuit impedance and reestablish the desired power input, where $V_{s,RMS}$ and $I_{s,RMS}$ are the power supply voltage and current, respectively, at the EAF transformer primary. In the case where the power input to the EAF transformer exceeds its rated power, the proposed series resistance controller works in conjunction with the electrode positioning controllers by inserting a percentage of the series resistance in the EAF secondary circuit to increase the speed of disturbance clearance. Since the electrical response is much faster than the mechanical movement of the electrode arms, the time of arc radiations on the refractories and cooling panels is decreased. The combined performance of the electrode position controllers along with series resistance compensation can therefore increase the ability of the regulators to reestablish, and maintain, the desired power input. Hence, it can avoid hot spots in refractories lining that can damage the EAF shell and cooling panels, interrupting production. In this way, the optimum power point is restored whilst satisfying the control constraints and without imposing large oscillations on the electrode arm mechanism.

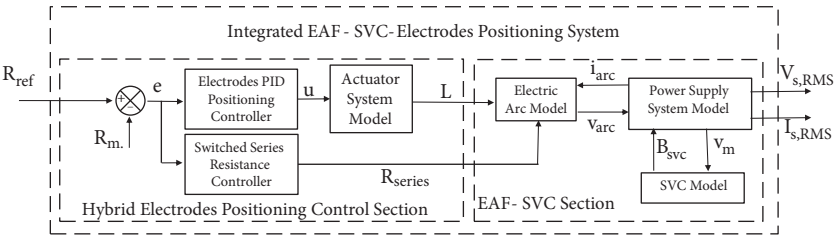

Figure 3. Sketch of new hybrid electrode-positioning systems technique.

3. EAF load characteristics

3.1. Power characteristics' curves of EAF

In order to calculate the electrical parameters that affect arc furnace operation and the arc furnace transformer power characteristics, the circuit impedance must be established. Using the generic equations in [14], the power circle diagrams of any EAF connected to the steel-making network can be deduced.

The following data from an actual steel plant are considered in Table 1 and Figure 4, respectively. Based on the calculated values, the optimum operating point for tap 10 (721 V) can be identified at P.F 0.87, 61 MW_{pri}, and 61 kA at the secondary side, as shown in Figure 5. This is the maximum point that the electrode positioner is to track for the EAF used in this study.

Table 1. Network data.

Point of common coupling $V_{(PCC\_PH-PH)}$ (kV)	220
Substation incoming feeders installed capacity (MVA)	3 × 380
Steel plant power transformers (kV)	220/33
Steel plant power transformers (MVA)	2 × 125/150 (ONAN/ONAF)
EAF transformers (Z%)	21%
EAF transformers (MVA)	4 × 58 MVA
EAF rated P.F	0.78
EAF transformer impedance at 58 MVA for 721 V	15.65%
EAF secondary impedance (mΩ)	0.4 + j2.4 mΩ
Ladle furnace capacity (MVA)	3 × 15 MVA
Minimum short circuit capacity (MVA_{SC_min})	8000
Maximum short circuit capacity (MVA_{SC_max})	15,000
System X/R Ratio	10
Thyristor-controlled reactors, MVA	265
Total harmonic filters, Mvar	250

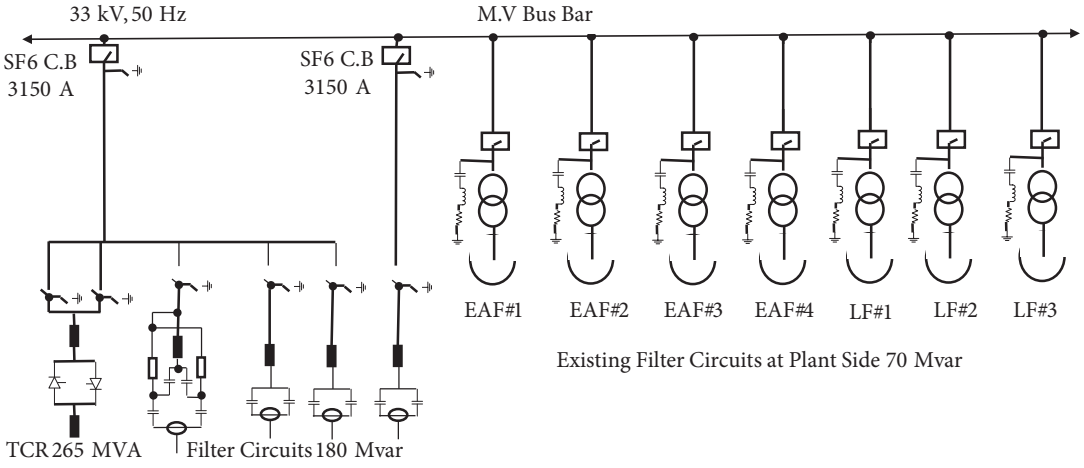

Figure 4. Single line diagram of 33 kV steel plant bus.

The dynamic relation between refractory wear index (RWI) and arc length is also expressed in Figure 6 according to Eq. (1). The importance of short arcs has been demonstrated in a number of published papers [15,16].

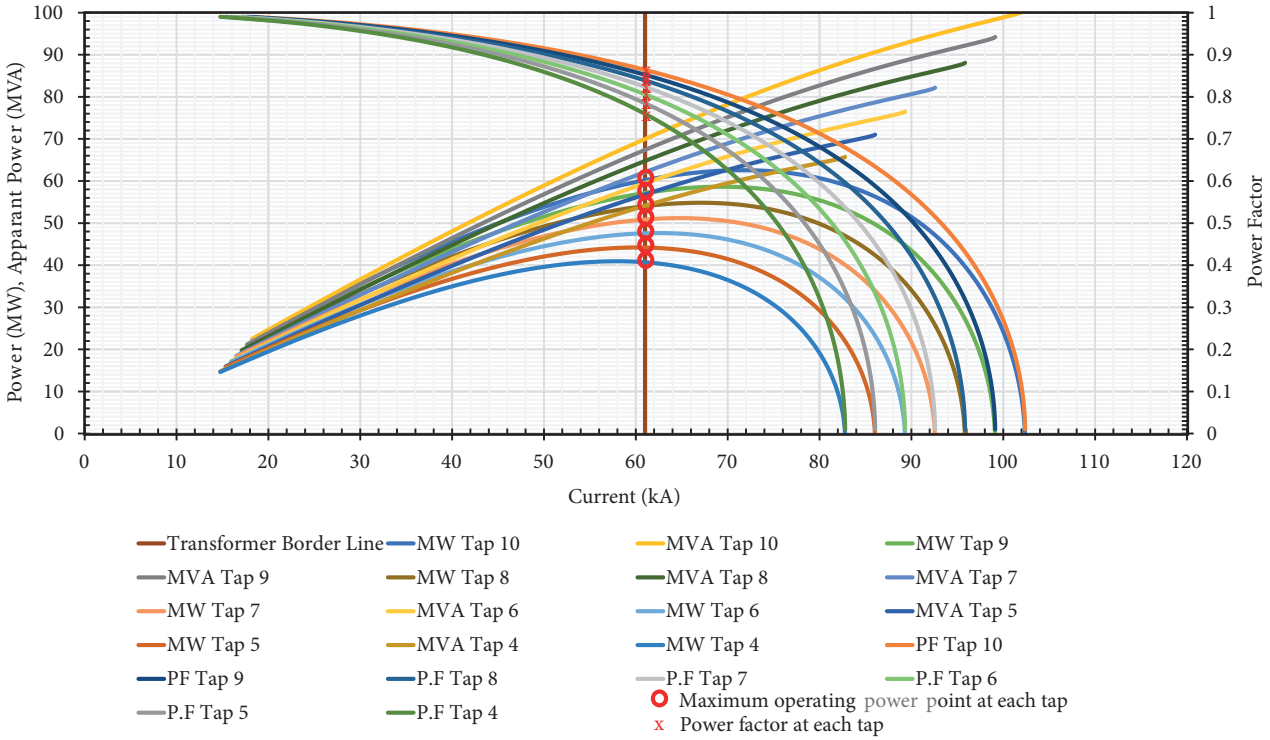

Figure 5. Dynamic characteristic power input curves for electric arc furnace operation.

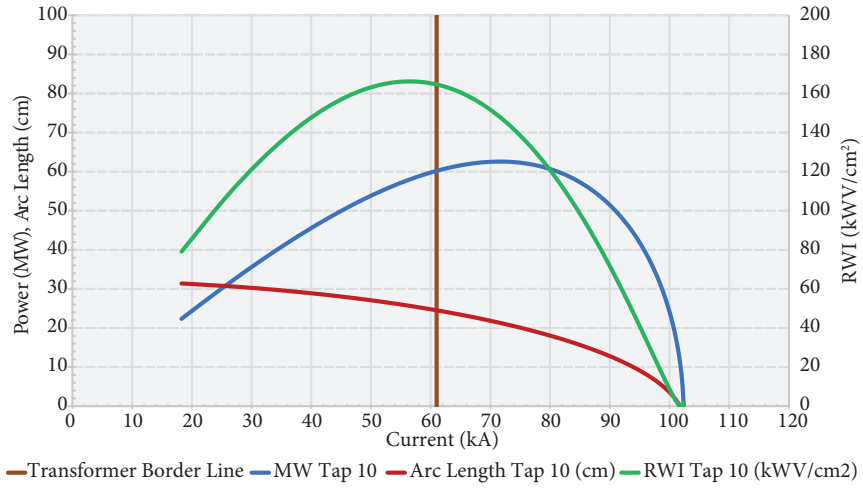

Figure 6. Dynamic characteristic showing RWI and arc length at Tap 10.

$$RWI(kWV/cm^2) = \frac{\text{arc power} \times \text{arc column volts} \times 1000}{3d^2}, \tag{1}$$

where d is the distance from outside of electrode to sidewall in centimeters (taken as 188 cm in this case), arc column volts = arc length $\times$ 12.

As shown in Figure 6, the RWI is 164 kWV/cm^2 at maximum operating point (61 kA, 61 MW, 24.3 cm arc length), while the RWI is 166 kWV/cm^2 at reduced operating point (56 kA, 57.6 MW, 25.7 cm arc length).

This demonstrates that keeping track of the maximum operating point is useful in terms of the refractory wear, as the arc length is reduced near the maximum operating point and hence the RWI is also reduced.

In order to understand the dynamic relation between electrode consumption and different operating points, first the mechanism of the graphite electrode consumption needs to be defined, as it falls into two basic categories termed continuous consumption and discontinuous consumption. Continuous consumption is defined as losses due to tip sublimation and sidewall oxidation. Discontinuous consumption is due to various forms of breakage, butt losses, and spalling. The calculations for continuous electrode consumption according to Jaccard (Effects of E.A.F. design and operation on electrode consumption, http://www.jaccard.com.br/EN/consumo.htm) are as follows:

$$C_{Tip}=R_{Sub}\times\frac{I^2\times\text{on tap time}}{Pr}, \tag{2}$$

where C_{Tip} is the graphite sublimation (kg/t),
R_{Sub} is the graphite sublimation rate (kg/kA^2-h),
I is the electrode current per phase (kA),
on-tap time is the heat time duration (h),
Pr is the EAF productivity in t/heat.

$$C_{side}=R_{ox}\times\frac{A\times\text{ tap to tap time}}{Pr}, \tag{3}$$

where C_{side} is the graphite oxidation (kg/t),
R_{ox} is the graphite oxidation rate (kg/cm^2-h),
A is the oxidizing electrode surface area (cm^2),
tap-to-tap time is the heat time duration in addition to work-around and delays time (h),
Pr is the EAF productivity in t/heat.

$$C\text{total}=C_{Tip}+C_{side}, \tag{4}$$

where C_{total} is the total electrode consumption in kg/t.

The on-tap time can be calculated from the following equation:

$$\text{On-tap time (minutes)}=\frac{\text{kWh/ton}\times\text{EAF capacity (tons)}\times 60(\text{min})}{\text{Active Power }(kW)\times EAF\text{ efficiency}\times\text{ EAF Equi. Availability}} \tag{5}$$

The operating values and dynamic characteristics are shown in Table 2. Similar results for a 54 MVA-rated EAF from [15] are shown in Table 3 for comparison.

Electrode consumption at maximum power point at tap 10 is less than tap 8 by 0.2 kg/t. That means 16.3 kg/heat and 350.77 kg/day lower electrode consumption for one EAF only. This demonstrates that successful operation at maximum power point at tap 10 is also beneficial in terms of electrode consumption, as a higher voltage tap is desirable to reduce current passing through the electrodes and hence the electrode consumption. The information obtained in this section will be useful for the simulation and control of the EAF, as will be illustrated later.

3.2. Dynamic–chaotic V–I characteristics of EAF

To model the dynamic V–I characteristics of EAF, few chaos-based models reported in specialized literature have been applied to simulate AC and DC arc furnaces [14]. The development of the general dynamic arc model

Table 2. Dynamic characteristics values.

Operation parameters	Operating values
KWh/t	562.6
EAF capacity (t)	81.5
Active power (MW)	61
EAF efficiency %	94
EAF equipment availability %	96.5
Turn-around and delays time (min/heat)	16.2
On-tap time at tap 10 (min)	50.3
On-tap time at tap 8 (min)	56.1
# Heats/EAF at tap 10	21.52
# Heats/EAF at tap 8	19.91
R_{sub} (kg/KA^2-h)	0.0233
R_{ox} (kg/cm^2-h)	0.00193
Oxidation area A (cm^2)	46,181.4
Total electrode cons. at tap 10 (kg/t)	2.1
Total electrode cons. at tap 8 (kg/t)	2.3

Table 3. Comparison between similar furnace parameters with different impedance power sources from [15].

Operation reactance, $\Omega \quad \times 10^{-6}$	3188	3866
Arc-power variation, MW (from 37.6 to 36.6 MW)	1	1
Current range, kA	54–69	48–63.5
Arc length, cm	16–12	18.5–13.3
Power factor	0.82–0.68	0.82–0.67
Refractory-wear index, kWV/cm^2	71–44	81–60

in the form of a differential equation is based on the principle of conservation of energy. The power balance equation for the arc can be expressed according to [14]. The typical steelmaking arcing cycles starts first with the arc ignition period, then the boring period, molten metal formation, the main melting period, the meltdown period, and finally the meltdown heating period, as illustrated in Figure 7. The complete set of combination of these parameters for different stages of electric arc can be found in [14].

3.3. SVC system characteristics

3.3.1. SVC dynamic characteristics

In this section, SVC model integration with EAF is presented. In the simulation and results section of this paper, the simulated results are compared with actual field data to validate the proposed model. Fourier analysis is used to derive the fundamental component of the thyristor-controlled reactor (TCR) susceptance B_{TCR} (α) that is given as [17]

$$BTCR(\alpha) = B\max(1\frac{2\alpha}{\pi} - \frac{1}{\pi}\sin 2\alpha) \tag{6}$$

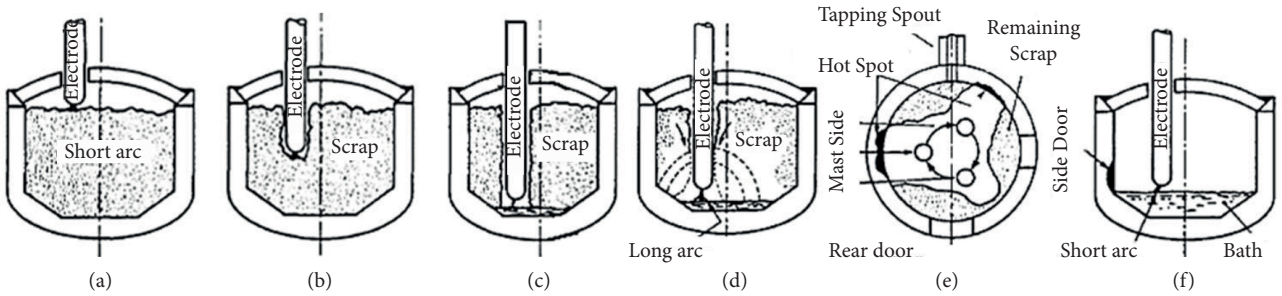

Figure 7. Typical steelmaking cycle: (a) arc ignition period (start of power supply), (b) boring period, (c) molten metal formation period, (d) main melting period, (e) meltdown period, (f) meltdown heating period.

$$B_{\max} = \frac{1}{\omega L}, \frac{1}{\pi} \sin 2\alpha) \tag{7}$$

where ϖ is the angular frequency of supply voltage,
L is the inductance of the TCR,
and α = the firing angle measured from positive going zero crossing of the applied voltage.

The firing angle α is related to the conduction angle σ, as follows:

$$\alpha + \frac{\sigma}{2} = \pi \tag{8}$$

3.3.2. SVC dynamic characteristics with voltage control

The compensator voltage control can be simplified as shown in Figure 8. The system voltage is measured, and the feedback system varies B_{TCR}. This results in reactive power equilibrium and therefore minimum voltage variation and flicker [1].

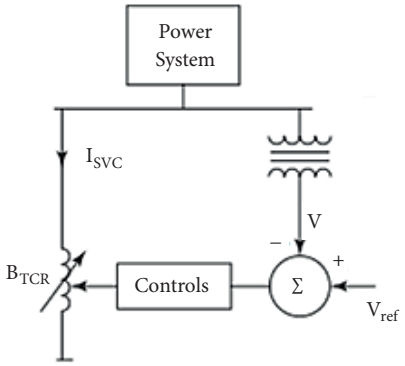

Figure 8. The operating characteristics of a TCR with voltage control.

4. Novel hybrid series compensation–impedance control method of electrode positioning system

4.1. Introduction

The technique currently used worldwide to maintain this maximum operating point during most of the heat time is to select the suitable voltage tap by a skilled operator and then hand over the fast dynamic control to the

electrode-positioning control during the main melt time. Obviously, this method is dependent, to some extent, on two main factors: operator experience in selecting the suitable voltage tap and electrode positioning control performance. Several recent studies have tried to apply intelligent controllers and neural recognition techniques to optimize the tap selection techniques [7]. Others are trying to replace the tap selection technique itself, with all its operational and maintenance problems, by applying flexible AC transmission systems (FACTS) to an inserted series reactor between substation transformer and EAF transformer, such as in [9,11].

The proposed control method explained in the next section is to take the constraints of EAF transformer power rating, increased I^2R losses, excessive localized refractory erosion, or hot spots into consideration to mitigate existing drawbacks in the conventional electrodes positioning systems explained in [8] by applying FACTS to series power resistance inserted in the EAF secondary circuit.

4.2. Schematic diagram

The details of the proposed hybrid series compensation–impedance control are shown in Figures 3 and 9, respectively. During normal operation, the proportional-integral–derivative (PID) electromechanical actuator is the dominant controller and the firing angle of the thyristors parallel to the compensated resistance equals 0°, creating resistance in the electrical circuit. During momentary short circuits, the firing angle is increased linearly towards 180° to compensate for the disturbance. The new series compensation method consists of a basic single-phase series resistance branch composed of an antiparallel-connected pair of thyristor valves, T_1 and T_2, in parallel with a linear resistance. The control range for the secondary circuit resistance from the power circle diagrams in Figure 5 ranges from 20 milliohms till 5.6 milliohms for tap 10 (721 V). In this case, the full range of the series resistance selected is 19.6 milliohms corresponding to firing angle of 180°.

5. Modeling and simulation results

5.1. MATLAB Simulink model of EAF

Using a numerical approach of the Simulink blockset, the dynamic voltage–current characteristic of the electric arc are modeled as shown in Figure 10. This model is then combined with the band limit white noise to create the chaotic nature of the arc furnace voltage and current parameters as shown in Figure 11.

5.2. MATLAB Simulink model of SVC

Based on the model built in the MATLAB environment in [14], the SVC control system can be simulated after parametrizing the network data to the discussed network parameters, as per Table 1. The SVC-simulated reactions to regulate the voltage are illustrated in Figure 12, which shows the reaction of the reactive power and voltage in response to SVC susceptance variation with firing angle. First, from $t = 0$ s to $t = 1$ s, the SVC is disconnected from the network and the thyristors are in full conduction (α is near 90°). Thus, the SVC susceptance is zero, the SVC is neither absorbing nor injecting reactive power to the network, and the voltage profile is near 0.8 pu due to existing connected inductive EAF loads. At $t = 1$ s, the SVC is connected to the network and hence the firing angle reacts by injecting capacitive reactive power to the bus (α moves toward 180°) to achieve reactive power equilibrium and restore the voltage profile to unity as shown. Similar actual network interactions are shown in Figure 13 regarding voltage profile (in blue) when SVC is switched on at 1200 hours to achieve reactive power equilibrium with EAF loading (in red). Table 4 shows the actual comparison between operation planned figures and actual results extracted from a steel-making plant daily report with almost the same operating conditions.

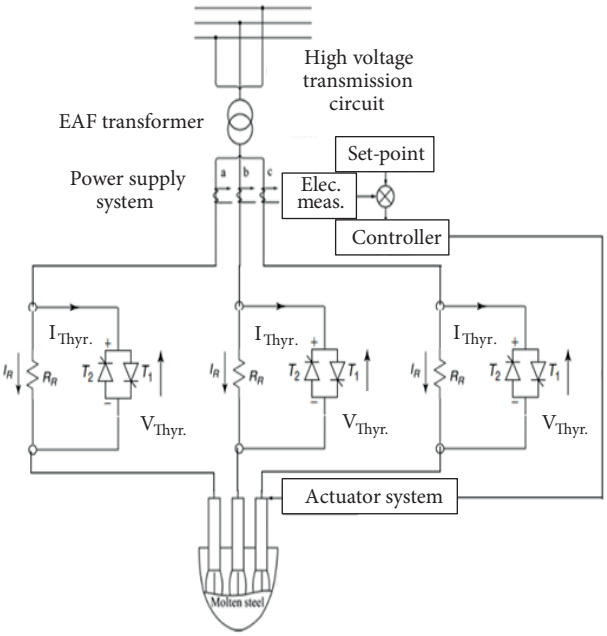

Figure 9. Schematic diagram of new hybrid electrode systems.

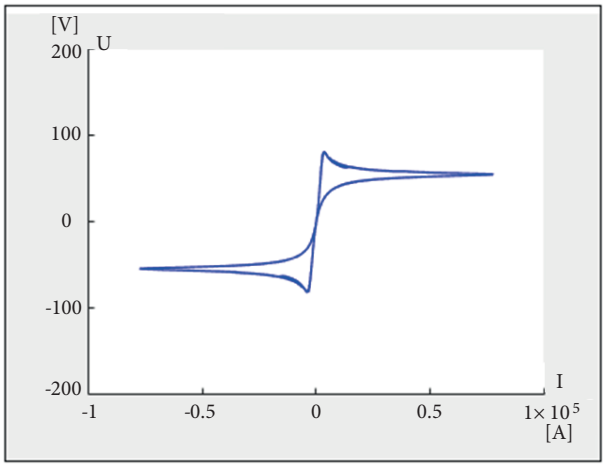

Figure 10. Dynamic characteristics of EAF.

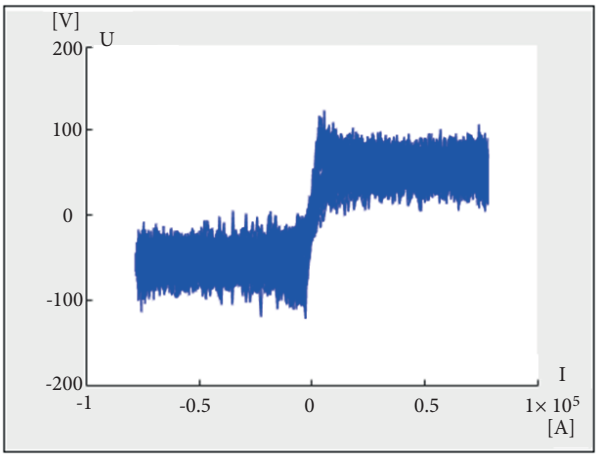

Figure 11. Chaoticdynamic characteristics of EAF.

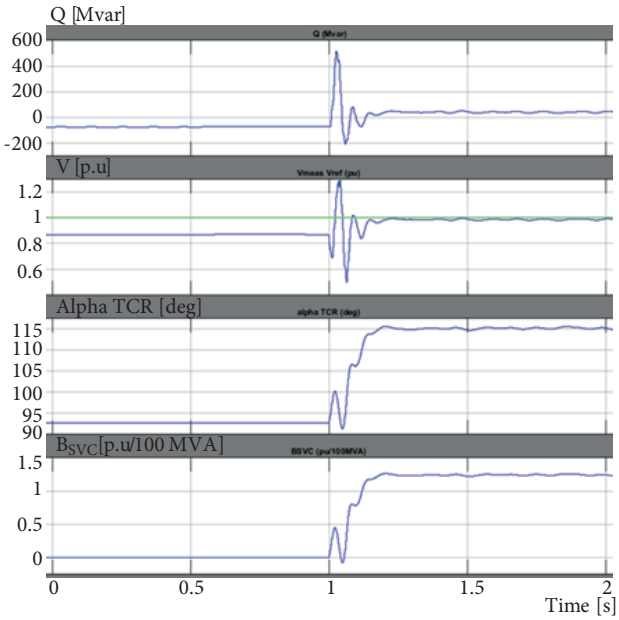

Figure 12. SVC interaction with power network dynamics.

5.3. Hybrid series compensation–impedance control model

In order to study the performance of the new control method, first the components of the electrode position controllers are demonstrated (Figure 14), which consist in this case study of an electromechanical winch drive

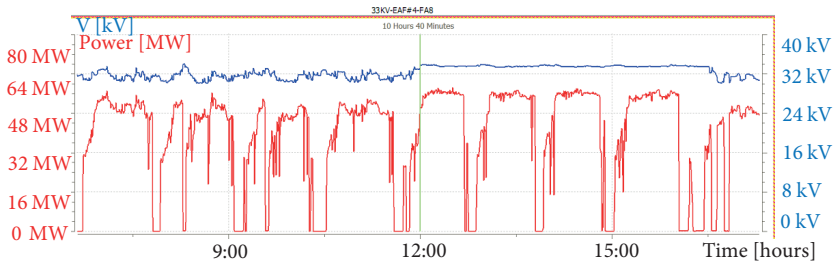

Figure 13. The 33 kV voltage profile with and without SVC operation from plant SCADA.

Table 4. Actual comparison between SVC in and out of service for same operating conditions.

Parameter	Planned figures	Without SVC in operation	With SVC in operation
Tapping yield %	87.3	86.3	87.3
Availability %	96.5	96.6	96.5
Direct reduced iron %	70	64.8	65.6
On-tap time (min/heat)	50.3	59.7	54.7
Turn-around and delay time (min/heat)	16.2	12.8	16.2
EAF power KWH/T	562.6	573.42	562.6
# heats/EAF	21.52	19.25	20

mechanism. The complete set of dynamic equations for the used electromechanical actuating system can be found in [8]. Some other electrode positioning systems use hydraulic actuating mechanism; for such systems dynamic equations can be found in detail in [18].

Each of the three electrodes is connected to its own actuator system, which acts according to the error input signal, to move it up or down. The described electromechanical system consists of a DC motor drive, a gearbox, and a winch. The winch motor linear no-load speed is 3250 rpm, equivalent to 162.5 mm/s (RPM/60 $\times$ wire diameter). The rated motor speed is 2375 rpm, equivalent to 118.75 mm/s. The DC motor is controlled using pulse width modulation and an H-bridge. The reference impedance is transferred into the position control signal. The PID position controller is tuned for optimum response and the output of the position controller is then fed to the speed controller. The speed controller is fed back with the actual speed to account for actual speed variations due to load disturbances. Disturbances of -500 N and $+500$ N at $t = 2$ s and $t = 3$ s, respectively, are simulated as shown in Figure 15, where the positioner controller is tracking a resistance value of 5.6 milliohms. At $t = 2$ s, an electrode breakage that would increase arc resistance is simulated. Accordingly, the electrode positioner gives a control signal to lower the electrodes arms down to clear the disturbance and restore reference value. At $t = 3$ s, a momentary short circuit is simulated, causing arc resistance to decrease. Accordingly, the electrode positioner gives a control signal to raise the electrode arms up to clear the disturbance. An actual similar behavior for the positioner controller from EAF supervisory control and data acquisition (SCADA) is shown in Figure 16 during a complete heat to compare between actual and simulated positioner controllers' reactions to disturbances. The electrode positioner reacts to electrode breakage and momentary short circuit disturbances to keep the 5.6 milliohms reference value as simulated.

The proposed series compensator control consists of a PID regulator and a firing unit. The thyristor tower and the power resistances are to be placed in series with the EAF transformer secondary circuit. Each

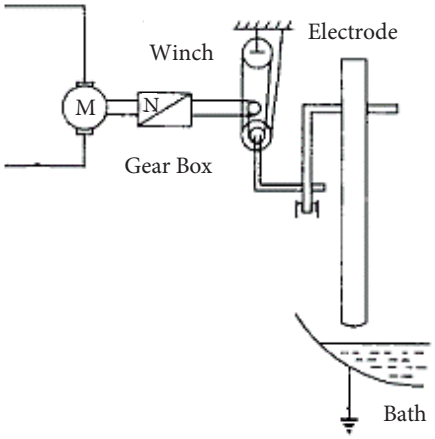

Figure 14. Electromechanical electrode-positioning controllers system components.

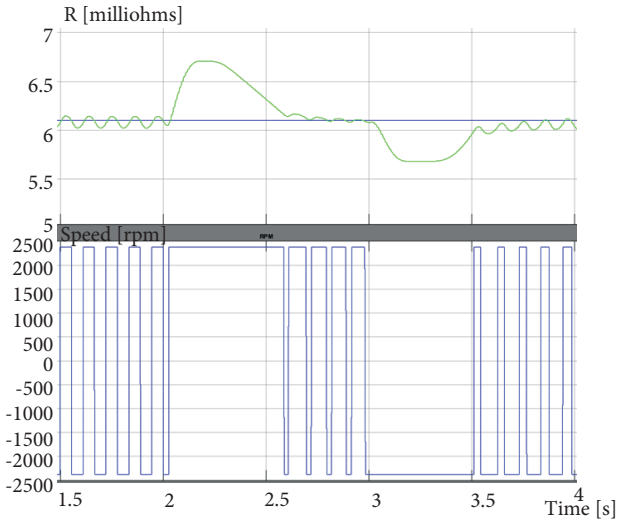

Figure 15. Tuned response of PID position controller.

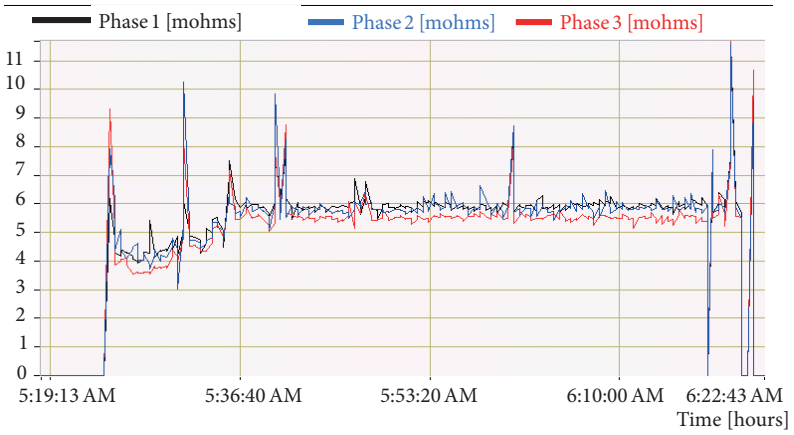

Figure 16. Actual response of PID position controller.

electrode phase has a series resistance with a back-to-back thyristor to control the percentage of compensation needed. Commercially available thyristor types and arrangements have been proposed in [11].

The tuned responses of the controllers to –500 N and +1000 N disturbances at $t = 2$ s and $t = 3$ s, respectively, are demonstrated in Figure 17. The overall series impedance response during momentary short circuits at $t = 3$ s (in red) is the superposition of the conventional position controller (in magenta) and the series resistance (in cyan).

The overall performance during a momentary short circuit at $t = 3$ s (red) is highly enhanced compared to the performance of the sole mechanical controller (magenta). The combined response restored reference impedance 2.5 s faster for the +1000 N disturbance (equivalent to 45 mm mast disturbance).

It worth noting that even though the tuned response is twice as fast as the untuned one (rise time 0.1 s instead of 0.2 s and settling time is 1 s instead of 2.7 s), both PID controllers are still much slower than the

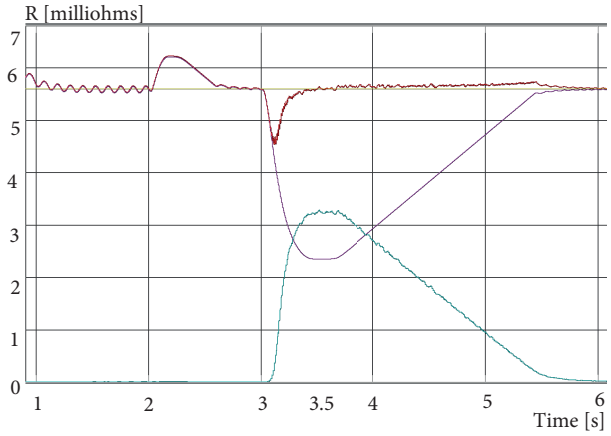

Figure 17. The overall series impedanceposition controller response (red); tuned conventional position controller response (magenta); and series resistance controller response (cyan).

combined response with series resistance. This is due to the mechanical bottleneck of the electrode-positioning system.

Figures 18 and 19 show the EAF simulated secondary current and secondary voltage in response to –500 N and +500 N disturbances at $t = 2$ and $t = 3$, respectively.

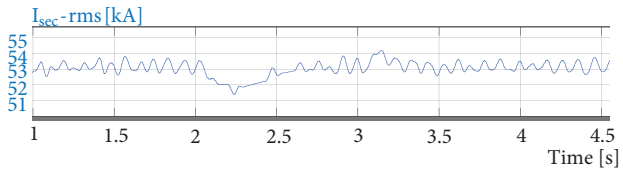

Figure 18. EAF secondary rms current.

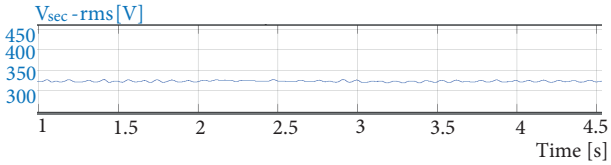

Figure 19. EAF secondary rms voltage.

Momentary short circuits are hardly noticed at $t = 3$ s, compared to the same disturbance at $t = 2$ s, due to series compensation, which results in better tracking for the optimum operating point. In addition, decreasing the duration of momentary short circuits is beneficial in terms of rate of electrode consumption and rate of refractory lining repair. The probability of damage to the furnace shell is also decreased, as the momentary short circuits are relieved more rapidly. The arc voltage and the arc current from the actual steel plant's EAF SCADA are shown in Figures 20 and 21 to show actual similar behavior compared to the simulated arc voltage and arc current reactions in Figures 18 and 19, respectively.

6. Conclusion

Generic modeling and integrated simulation of a steel making EAF-SVC-electrode positioning systems are realized using the MATLAB Simulink environment and validated using trends collected from an actual steel plant.

A new concept of electrical series compensation is introduced for the first time in this paper. It enhances conventional impedance control and results in mitigations of momentary short circuits that are 2.5 s faster than conventional impedance control methods without imposing large oscillations on electrodes positioner mechanism, as illustrated in Figures 17, 19, and 20.

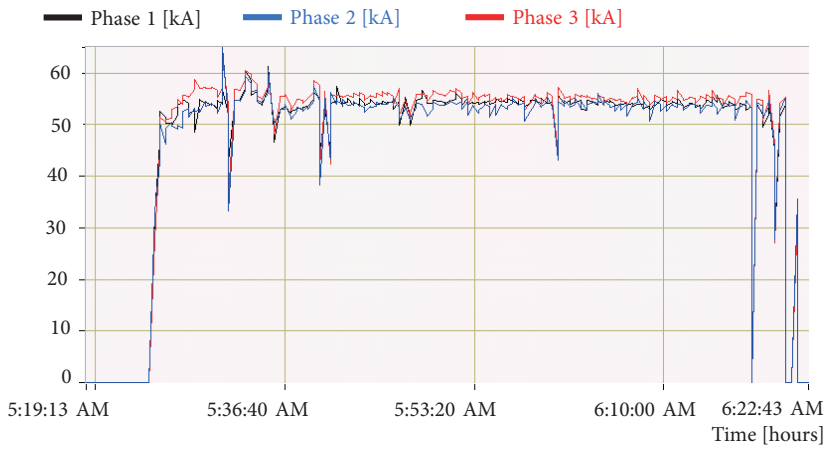

Figure 20. EAF arc current from plant SCADA.

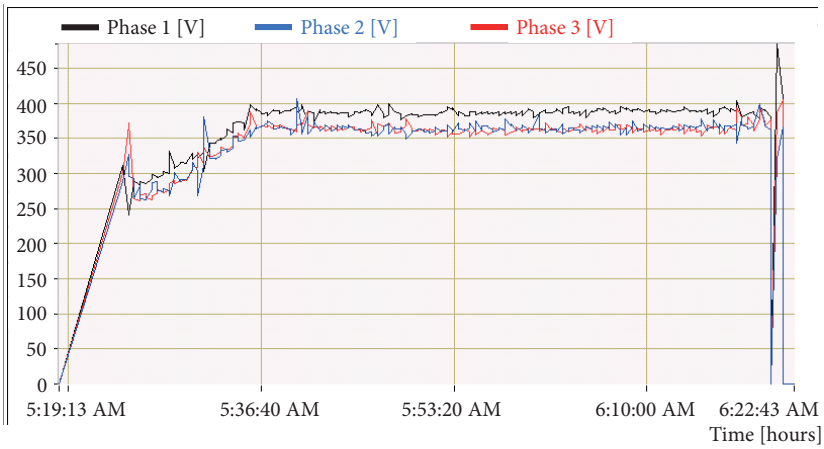

Figure 21. EAF arc voltage from plant SCADA.

The expected benefits of the proposed hybrid control method should easily be reflected in lower electrode consumption, better tracking of maximum power transfer, lower refractory hot spots, and lower on-tap time, which means higher number of heats. Further analysis concerning the extent of benefits from applying this method, especially on electrode consumption, refractories, and heat time, can be investigated in future work concentrating on the technoeconomic results of a developed prototype.

References

[1] Hasani R, Azad I. Design optimal controller for reduce voltage flicker and harmonic distortion in power system base on SVC. International Journal of Engineering and Innovative Technology (IJEIT) 2013; 3: 540-544.

[2] Spasojević L, Papič I, Blažič B. A new approach to the modelling of electric arc furnaces with representative voltage samples. Int T Electr Energy 2014; 25: 1173-1186. DOI: 10.1002/etep.1895.

[3] Chang GW, Shih MF, Chen YY, Liang YJ. A hybrid wavelet transform and neural-network-based approach for modelling dynamic voltage-current characteristics of electric arc furnace. IEEE T Power Deliver 2014; 29: 815-824. DOI: 10.1109/TPWRD.2013.2280397.

[4] Samet H, Mojallal A, Ghanbari T. Employing grey system model for prediction of electric arc furnace reactive power to improve compensator performance. Prz Elektrotechniczn 2013; 12: 110-115.

[5] Janabi-Sharifi F, Jorjani G. An adaptive system for modelling and simulation of electrical arc furnaces. Control Eng Pract 2009; 17: 1202-1219.

[6] Hauksdottir AS, Soderstrom T, Thorfinnsson YP, Gestsson A. System identification of a three-phase submerged-arc ferrosilicon furnace. IEEE T Contr Syst T 1995; 3: 377-387.

[7] Raisz D, Sakulin M, Renner H, Tehlivets Y. Recognition of the operational states in electric arc furnaces. In: The IEEE 9th Conference on Harmonics and Quality of Power; 1–4 October 2000; Orlando, FL, USA: IEEE. pp. 475-480.

[8] Billings SA, Nicholson H. Modelling a three-phase electric arc furnace: a comparative study of control strategies. Appl Math Model 1977; 1: 355-361.

[9] Pires IA, Cardoso MMG, Filho BJC. An active series reactor for an electric arc furnace: a flexible alternative for power-flow control. IEEE Ind Appl Mag 2016; 22: 53-62.

[10] Haidar S, Ghanbari T, Ghaisari J. Maximum performance of electric arc furnace by optimal setting of the series reactor and transformer taps using a nonlinear model. IEEE T Power Deliver 2015; 30: 764-772.

[11] Cardoso MMG, Filho BJC. Thyristor switched series reactor for electric arc furnaces. IEEE Ind Applic Soc 2006; 1: 124-130.

[12] Bosi F. Electric steelmaking. In: Electric Steelmaking Course of the Brazilian Association of Metallurgy and Materials. ABM 2004.

[13] Bowman B. Effects on furnace arcs of submerging by slag. Ironmak Steelmak 1990; 17: 123-129.

[14] Hassan AM, Abou-Ghazala A, Megahed A. Mitigation of steel making plants' electrical power quality problems using SVC – A case study. Prz Elektrotechniczn 2016; 7: 121-127. DOI:10.15199/48.2016.07.27.

[15] Shawabe WE. Ultra high power furnaces. Iron Steel Eng 1969; 46: 132-137.

[16] Freeman ER, Medley JE. Efficient use of power in electric arc furnaces. Electric Power Applications 1978; 1: 17-24.

[17] Mathur RM, Varma RK. Thyristor-Based Facts Controllers for Electrical Transmission Systems. Hoboken, NJ, USA: John Wiley & Sons, Inc., 2002.

[18] Wang Y, Mao ZZ, Tian HX, Li Y, Yuan P. Modeling of electrode system for three-phase electric arc furnace. J Cent South Univ T 2010; 17: 560-565. DOI: 10.1007/s11771-010-0523-3.